Reconstructions of 3D Coronal Electron Density from Solar Minimum to Maximum of Solar Cycle 24 by Improved Tomography

Tongjiang Wang[1,2], Shaela I., Jones[1,2], C. Nick Arge[2]

([1]The Catholic University of America; [2]NASA's Goddard Space Flight Center)

1. Introduction

Tomography is a powerful tool for reconstructing the three-dimensional (3D) density structure of the global solar corona, providing critical insights into the interplay between magnetic and plasma structures, the connection of solar wind streams to the lower solar atmosphere, and inner boundary conditions for solar wind models.

In this study, we introduce an enhanced tomography technique incorporating radial weighting in the regularization term. This approach balances smoothing across different heights, enabling the recovery of finer density structures at lower heights while stabilizing solutions and minimizing oscillatory artifacts at greater heights.

Using this method, we generated a comprehensive database of 3D coronal electron density for Carrington Rotations (CRs) 2052 to 2154, spanning the period from January 8, 2007, to September 17, 2014, using pB images from STEREO/COR1B, which is now available in STEREO Science Center (SSC) archive.

Comparison of reconstructions for CR 2091 using single-satellite versus multi-viewpoint data reveals that coronal evolution and dynamics substantially influence the reconstructed density structures.

We highlight its versatility in advancing our understanding of the solar corona and emphasize the importance of 3D coronal density reconstructions in enhancing the accuracy and applicability of solar wind models (e.g., the WSA model) for space weather forecasting (e.g., Jones et al. 2022).

2. Tomographic Reconstruction

- **Method**

$$pB(\rho) = \int_{\text{LOS}} K(\rho, r) N(s) ds \quad \Rightarrow \quad \boldsymbol{Ax = y}$$

Where $\mathbf{x}=[x_1, x_2, \ldots x_n]^T$ is unknow density, $\mathbf{y}=[y_1, y_2, \ldots, y_m]^T$ is data, and Matrix **A** contains the known coefficients depending on the geometries and Thomson scattering.

- **Solving Linear Problem with Regularization**

(Frazin & Janzen 2002; Kramar +2009)

$$\min_{\mathbf{x}} F = \|\boldsymbol{Ax - y}\|^2 + \mu \|\boldsymbol{Rx}\|^2$$

$$\Leftrightarrow F = \frac{1}{2}\boldsymbol{x}^T \boldsymbol{M x} - \boldsymbol{b}^T \boldsymbol{x}$$

where $\boldsymbol{M}=\boldsymbol{A}^T\boldsymbol{A} + \mu \boldsymbol{R}^T\boldsymbol{R}$ and $\boldsymbol{b}=\boldsymbol{A}^T\boldsymbol{y}$. This quadratic function can be minimized by conjugate gradient (CG) method by iteration.

- $\|\boldsymbol{Rx}\|^2$ represents the smoothing of the solution, e.g., L2 norm of 1st order or 2nd order derivatives. Regularization term is used to reduce the noise effect and make the solution stable and unique.
- μ is the regularization parameter, controlling the trade-off between the fidelity to the data and the regularization term. This parameter can be optimized by cross validation (CV)

- **Improving by Weighting Factor in Regularization**

$$F_2^w = \|\boldsymbol{R}^w \boldsymbol{x}\|^2 = \sum_{i',j',k'} w^2(r_{i'}, j', k') \left[\left(\frac{\partial^2 f}{\partial u^2}\right)^2_{i',j',k'} + \left(\frac{\partial^2 f}{\partial v^2}\right)^2_{i',j',k'} + \left(\frac{\partial^2 f}{\partial w^2}\right)^2_{i',j',k'} \right]$$

We apply a weighting factor $w=1/N_{bg}(r)$ or $w=1/I_{bg}(r)$ in the regularization term, where $N_{bg}(r)$ is the radial background density obtained using the SSPA method (Wang+2017), $I_{bg}(r)$ the background pB. This radial weighting helps achieve balanced smoothing across different heights, allowing for the recovery of finer structures at lower heights while stabilizing the solution and preventing oscillatory artifacts at higher altitudes.

3. Applications for STEREO/COR1 pB Observations

- **Single-Spacecraft Reconstruction**
  - Data Preparation
    1) Collecting data over approximately half of a solar rotation
    2) Sampling *pB* images at 12-hour intervals → ~ 27 – 28 images
    3) Despike processing, then rebinned to a 128×128 format
  - Inversion
    1) In the Cartesian grid, a 128^3 grid in Carrington coordinates is used with a spherical domain $R_{in}-2ds \le r \le R_{out}+2ds$, where R_{in} =1.5 $R_\odot$ and R_{out} =4.0 $R_\odot$
    2) In the spherical grid, a 361× 181× 51 grid in the longitudinal, latitudinal, and radial directions is used, with inversion in $R_{in} \le r \le R_{out}$, with data sampling consistent with the Cartesian grid case.

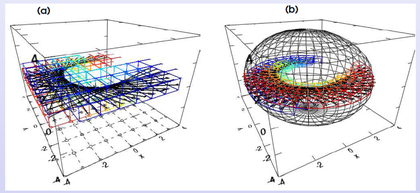

Fig.1: Illustration of reconstruction in (a) Cartesian grid and (b) spherical grid. The 28 rays, corresponding to a given data point in 28 successively observed images over two weeks by COR1-B, are shown as black lines, while the intersected cells are indicated by colored lines.

- **Example for Reconstruction of CR 2098**
  - Left panels of Figure 2 demonstrate the 3D electron density reconstruction for CR 2098 using the improved tomography with weighting factor w= $N_m/N_{bg}(r)$ and a second-order smoothness.
  - The green contours indicate some regions with negative-density artifacts, likely resulting from the ill-posed nature of tomography (e.g., variations in data and noise cause the instability of solution).
  - Right panels show a comparison of its 3D density with that of MHD steady solution modeled by PSI, using MDI magnetic data over the whole CR.

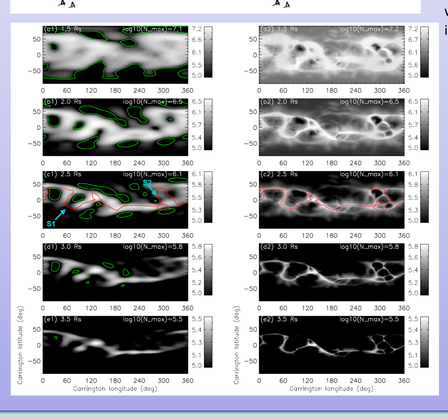

Fig.2: Comparison of 3D coronal density for CR 2098 using radially-weighted tomography with μ = 0.3 (Left panels) and that obtained from the MHD simulation (Right panels). The green contours indicate the regions of non-positive values. In Panels (c1) and (c2), the red contours represent the magnetic neutral line for the radial component of the magnetic fields in the MHD model.

4. Error Analysis and Validation

- **Reconstruction Errors**
  - By calculating the standard deviation of the average of *5*-fold solutions generated through cross-validation, the relative errors are estimated to be 5.1%, 1.4%, 1.9%, 2.6%, and 4.2% at 1.5, 2.0, 2.5, 3.0, and 3.5 $R_\odot$, respectively.
  - Figure 3 compares the globally-averaged radial profiles of electron density distributions for three cases. The tomographic solutions show a tendency for density increasing near the outer boundary due to a finite computational domain.
  - Applying radial weighting helps reducing over-smooth near the inner boundary, making it better consistent with that of the MHD model.

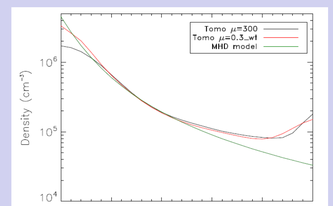

Fig.3: Radial distributions of the globally-averaged coronal electron density for the tomographic reconstructions in different cases:

Black lines: without radial weighting

Red lines: with radial weighting

Green lines: the MHD model from PSI

- **Zeroth-Order Regularization**

$$\min F = \|\boldsymbol{Ax - y}\|^2 + \mu \|\boldsymbol{x}\|^2$$

  - Since zeroth-order smoothness is the simplest regularization, we examine whether this smoothness can recover more finer density structures.
  - Figure 4 compares the results with and without radial weighting factor in regularization. Both solutions show the density structures comparable to the case with second-order smoothness.

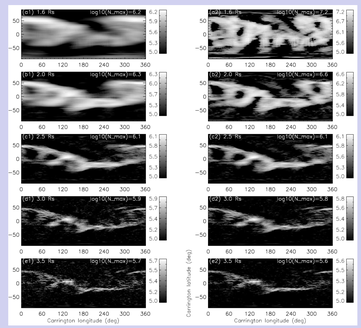

Fig.4 Comparison between the 3D coronal densities for CR 2098 reconstructed by tomography using zeroth-order regularization.

Left Panels: without radial weighting.

Right Panels: with radial density weighting.

5. Effects of Temporal Evolution on Reconstruction

- **Constraints**
  - Since the solution is assumed to be static throughout the two-week data collection period from a single spacecraft, it should represent density structures that are either stable or evolving slowly enough to persist over that time.
  - To examine how the reconstruction changes with data collection time, Figure 5 compares the reconstruction of CR 2098 (Middle) with two control experiments: one using data collected a week earlier (Top), and the other collected a week later (Bottom).

- **Single-Viewpoint vs. Multi-Viewpoints**
  - The best approach to overcome the impact of density evolution is to apply multi-viewpoint reconstructions – inherent advantage of the tomography technique
  - By leveraging observations from STEREO/COR1-A, COR1B, and LASCO/C2 when they are separated by ~ 60°, the reconstruction only requires about 4-5 days. Figure 6 compares the reconstructions of CR 2091 between single-view (Top and Middle) and multi-views (Bottom). Distinct differences reveal significant changes of the corona.

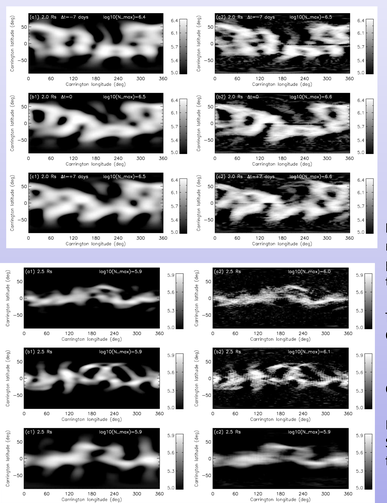

Fig.5: Comparison of 3D densities reconstructed for CR 2098 using pB images observed during three different periods:

Top Panels: 7 days earlier
Middle panels: 23 June to 7 July 2010
Bottom Panels: 7 days later

Left: second-order smoothness
Right: zeroth-order smoothness

Fig.6: Comparison of 3D densities reconstructed for CR 2091 from pB images using single satellite and three satellites.

Top panels: Using the data from COR1B during the first half of CR.

Middle panels: Using the data from COR1B for the second half of CR.

Bottom panels: Using the data from STEREO-COR1A, COR1B, and LASCO-C2 for 5 days, during the middle of CR.

6. Description of 3D Electron Density Product

- **Tomography Inversion Codes**

Tomography inversion codes in FORTRAN-90 on both Cartesian and Spherical grids have been developed and will be open to the public when this study is published (Wang+2025). Tests using STEREO/COR1 data show that the results produced by the two grids are in good agreement.

- **Data Archive for 3D Electron Density**

Using the code on a spherical grid of 361 × 181 × 51 in longitude, latitude, and radial direction with $I_{bg}(r)$ weighting in regularization, reconstructions of the 3D density in 1.5 $R_\odot$ < r < 4.0 $R_\odot$ for CRs 2052 to 2154 (two per CR) were calculated using STEREO/COR1B data, covering the period from 2007-01-08 to 2014-09-1. The dataset of these reconstructions, in the standard FITS format, is now available on the **STEREO Science Center (SSC) website:**

https://stereo-ssc.nascom.nasa.gov/data/ins_data/Secchi/N3D_COR1B_2024/

Acknowledgement:

The work of TW and SIJ has been supported by NASA Cooperative Agreement 80NSSC21M0180 to The Catholic University, Partnership for Heliophysics and Space Environment Research (PHaSER).

References:

Frazin, R.A., Janzen, P.: 2002, ApJ, 570, 408
Kramar, M., Jones, S., Davila, J., Inhester, B., Mierla, M.: 2009, Sol Phys., 259, 109
Jones, S. I., Wang, T. J., Arge, C. N., Henney, C.J., Uritsky, V.M., Rura, C.:, 2022, ApJ, 928, 131
Wang, T. J., and Davila, J. M.: 2014, Solar Phys., 289, 3723.
Wang, T. J., Arge, C. N., and Jones, S. I.: 2025, Solar Phys., submitted (This Study).